ORIGINAL RESEARCH

Remediation and Treatment

Adsorption of Direct Orange 46 and phosphate ions on waste tomato stem ash used as a bio-based adsorbent

Ozan Eskikaya[1] | Hudaverdi Arslan[1] | Melis Gun[1] | Raouf Bouchareb[2,3] | Nadir Dizge[1]

[1]Department of Environmental Engineering, Mersin University, Mersin, Turkey

[2]Department of Environmental Engineering, Process Engineering Faculty, Saleh Boubnider University, Constantine, Algeria

[3]Laboratory of Process Engineering for Sustainable Development and Health Products (LGPDDPS), National Polytechnic School of Constantine, Constantine, Algeria

Correspondence
Nadir Dizge, Department of Environmental Engineering, Mersin University, Mersin 33343, Turkey.
Email: nadirdizge@gmail.com

Abstract

It is necessary to use adsorbents derived from natural materials, such as biosorbents since they do not any damage to the environment, for pollutants elimination that contaminate the aquatic environment. Since the deficiency in the literature was determined in the study in which only the adsorbent obtained from tomato stem was used before this study, a waste material with tomato stem was selected as a natural adsorbent without chemical compounds. Phosphate and dye contaminants, which are often present in industrial and municipal wastewater, were eliminated by adsorption process. Fourier transform infrared (FTIR), x-ray fluorescence (XRF), Zeta potential, and scanning electron microscope (SEM) with energy dispersive x-ray (EDX) spectroscopy were used to analyze tomato stems. The tomato stems resulted in high pollutants removal efficiencies recording 99.31% of phosphate (PO_4^{3-}) removal efficiency and 99.44% of Direct Orange 46 (DO 46) dye removal efficiency at optimal conditions. The best conditions for phosphate adsorption were pH $= 6.0$, 2.0 g/L of tomato stems concentration, 50 mg/L initial phosphate concentration and a contact time of 120 min resulting in an adsorption capacity of 4.24 mg/g. The best conditions for DO 46 adsorption were pH $= 12$, 2.0 g/L of adsorbent concentration, initial dye of 200 mg/L concentration and a contact time of 120 min ($q = 13.76$ mg/g). For both adsorption experiments, the adsorbent size was chosen to be less than 500 μm. As a result of the adsorption experiments on tomato stem ash, Freundlich isotherm (R^2: 0.94) was suitable for DO 46 dye adsorption and Temkin isotherm (R^2: 0.99) was suitable for PO_4^{3-} elimination. The phosphate (R^2: 0.97) and dye (R^2: 1) adsorption onto tomato stem ash was explained using a pseudo-second-order kinetic model. It has been determined that the adsorption of the DO 46 dye with the tomato stem ash is an exothermic (ΔH: -3.174) process that occurs naturally due to its nature (ΔG: -8.41). On the other hand, it was determined that the adsorption of PO_4^{3-} was spontaneous (ΔG: -5.21) and endothermic (ΔH: 5.7357). According to the adsorption results obtained in this study, it is appropriate to use the tomato stem, which is generated as waste, as an adsorbent. It is thought that obtaining from bio-based waste in

1 | INTRODUCTION

Economic growth, urbanization, and population increase have a negative impact on environmental factors. Untreated wastewater, on the other hand, contaminates existing water resources and jeopardizes the supply of safe drinking water.[1] Hazardous organic–inorganic chemicals, persistent organic pollutants, and volatile pollutants, among other toxic components in wastewater, are dangerous to both the ecosystem and human health.[2] Phosphate (PO_4^{3-}) from organic contaminants is necessary for plant growth, but when phosphate levels in surface water surpass 25 μg/L, it can speed up the algal blooms growth and induce eutrophication. Eutrophication caused by algal overgrowth can deplete water self-cleaning capacity, cause damage on water systems and lower water quality.[3,4] Dyes, which are among the most harmful pollutants, are widely found in the wastewater of different industries, including textile processing,[5,6] paper, leather tanning, cosmetics, and pharmaceuticals. Dyes are classed as cationic, anionic, or non-ionic based on the charge of their dissolved particles in an aqueous media. Furthermore, colors are difficult to biodegrade[7–9] Pollutant removal from drinking water and municipal wastewater treatment plants is dependent on the contaminants physicochemical properties as well as the treatment procedures.[10] For this reason, many processes are used and developed for the treatment of wastewater such as coagulation-flocculation,[11,12] membrane,[13] photocatalytic,[14,15] electrochemical systems,[16,17] and adsorption.[18]

Adsorption is a physicochemical mass transfer event that occurs when a liquid is deposited or adsorbed on the surface of a solid phase.[19,20] Diffusion can move dissolved species to the pores of the adsorbent and/or to the inner surface of the adsorbent. Adsorbates are components that are surface-deposited, whereas adsorbents are the solid phases that hold the adsorbate. The efficiency of the adsorption process is closely related to the adsorbent's capacity to remove contaminants, which is influenced by factors including pH, temperature, the kind, and amount of material being adsorbed, the adsorbent's physical characteristics, and the liquid it comes into contact with.[21] Contaminants elimination by adsorption process has turned out to be the most economically valuable separation technology due to its simplicity, cheap cost compared to alternative treatment methods and respective to the environment. Adsorbents used to remove contaminants from wastewater have two primary factors that define their privilege in the industrial wastewater systems: low cost and high efficiency. Adsorbing capacity, pore structure, and active surface area are additional essential adsorbent features.[22,23] Adsorbents may be categorized into three groups for the removal of pollutants in wastewater: inorganic, organic and industrial by-products. The main criteria

determining the performance of an adsorbent before being used in a real wastewater system is its high efficiency at a reasonable cost.[24] Biosorbents generated from natural materials have the potential to be a viable alternative to inorganic ones. Agricultural waste, plant-based adsorbents, fungus, and bacteria are all examples of biosorbents. Plant-based cellulose biosorbents, in particular, have attracted attention because of their high absorption capacity, lack of toxic waste formation, low cost, flexibility of use and renewability.[25,26]

This study was aimed to purify phosphate and anionic dye (DO 46) in aquatic environment using a biosorbent obtained from tomato stem. A waste material including tomato stem was chosen as a natural adsorbent free of chemical compounds since the study that identified the gap in the literature prior to this investigation, in which only the adsorbent derived from tomato stem ash was employed. In adsorption experiments, the effect of wastewater pH value, initial pollutant concentration, amount and size of biosorbent on removal efficiency of dye and phosphate were investigated with adsorption capacity. The best conditions obtained within the parameters of the study were used to conduct adsorption isotherm, kinetic, and thermodynamic analyses. In addition, characterization analyzes of the obtained biosorbent were also performed.

2 | MATERIALS AND METHODS

2.1 | Synthesis of tomato stem ash for use as an adsorbent

In the agricultural region of Mersin, Turkey, throughout the summer, the leftover plant stems are gathered after the tomatoes have been picked. They were rinsed three times in a basin with distilled water to wash away any organic waste, grit, and dust. The washed tomato stems are first dried for 2 h in an oven at 70°C. Then, the dried long stems are shredded and powdered using a domestic grinding machine to obtain fine particles. To ensure a consistent heat process and powder particles of the same size during calcination, tomato stem powder was sieved using various mesh sizes before being put in a ceramic pot. After being calcined at 900°C for 2 h in a muffle furnace, the final obtained ash was used as biosorbent.

2.2 | Adsorption experiments using tomato stem ash

To investigate the pollutants sorption on tomato stem ash, the concentrations of different initial pollutants, the pH of the solution, the size and dosages of the adsorbents were the main topics of the
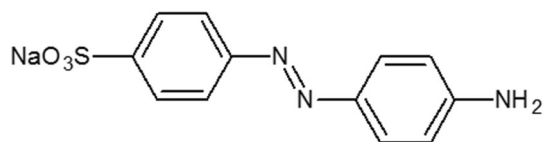
FIGURE 1 Molecular structure of DO 46 dye.

investigation. The pH was adjusted between a range of 2–12 using 0.1 M NaOH and 0.1 M HCl. To investigate how adsorbent size affects the efficiency of pollutant removal, three different sieve sizes—20, 30, and 35 mesh—were employed. The studied adsorbent concentration was changed between 0.5 and 2.0 g/L for optimal adsorbent size. Various amounts of PO_4^{3-} (from 10 to 75 mg/L) and dye (from 25 to 200 mg/L) were dissolved in distilled water. The adsorption tests were conducted in a shaker with a sample volume of 50 mL and a mixing speed of 150 rpm at room temperature. The samples were centrifuged (5 min and 6000 rpm) after the adsorption process to calculate the percentage of pollutant removed. The pollutants removal efficiencies were estimated using Equation (1) and adsorption capacities were estimated using Equation (2):

$$\text{Removal efficiency}(\%) = \left(\frac{Ci - Ce}{Ci}\right) * 100, \quad (1)$$

$$\text{Adsorpsion capacity}(q) = \left(\frac{Ci - Ce}{M}\right) * V, \quad (2)$$

where Ci and Ce (mg/L) refer to pollutants concentration before and after the treatment process, respectively; V (L) is the solution volume, and M (g) is the amount of adsorbent.

PO_4^{3-} content of the solutions using potassium dihydrogen phosphate ($KH_2PO_4^{3-}$) and an anionic dye DO 46 "DO 46" (Sirius Orange K-CFN) were obtained from Sigma Aldrich. Vanadomolybdophosphoric Acid Colorimetric Method was used for PO_4^{3-} analysis.[27] Figure 1 shows the DO 46 dye's chemical structure.

2.3 | Adsorption kinetic and isotherm studies

Adsorption isotherms, which are extremely important, may be used to predict how the adsorbent and adsorbate will interact. An adsorption isotherm, which defines an equilibrium relationship between the liquid concentration at constant temperature and the quantity of material adsorbed, is used to determine the extent of adsorption. Adsorption isotherms offer details about the adsorption mechanism and the interactions between adsorbent and adsorbate.[28] An adsorption kinetic consists of three phases. The adsorbate is first externally mass transferred from the bulk solution to the adsorbent's external surface (pseudo-first kinetic), then internally diffused to the sorption sites (pseudo-second kinetic), and lastly sorption (intraparticle diffusion). As a result, fitting to the models allows for the clarification of the adsorption mechanism.[29] Table 1 shows the isotherms and kinetics formulas for the tomato stem ash adsorption used in this study.

TABLE 1 The isotherms and kinetics formulas of the tomato stem ash for adsorption.

Kinetic	Formulas	Equations
Pseudo-first kinetic	$\log(q_e - q_t) = \log q_e - k_1 . t$	(3)
Pseudo-second kinetic	$\frac{1}{qt} = \frac{1}{k_2 . q_e^2} + \frac{1}{q_e} . t)$	(4)
Intraparticle diffusion	$q_t = k_i t^{0.5} + C$	(5)

where q_e and q_t are the adsorption capacities at equilibrium and time t (mg/g), respectively. k_1 is Lagergren constant (L/min), k_2 is the second-order constant (mg/g min), k_i is the intraparticle diffusion rate constant (mg g $\min^{1/2}$), C is the boundary layer thickness constant.

Isotherm	Formulas	Equations
Langmuir	$\frac{C_A}{q_A} = \frac{1}{b_A . q_m} + \frac{C_A}{q_m}$	(6)
Freundlich	$\log(q_A) = \log(K_F) + \frac{1}{n} \log(C_A)$	(7)
Dubinin–Radushkevich (D–R)	$\ln q_A = \ln q_s - K_{ad} \left[RT \ln\left(1 + \frac{1}{C_A}\right)\right]^2$	(8)
Temkin	$q_A = \frac{RT}{b_T} \ln A_t + \frac{RT}{b_t} \ln C_A$	(9)

where C_A is the concentration of adsorbate A at the equilibrium (mg/L), b_A is the Langmuir constant for the adsorbate A (L/mg). q_m is the adsorbent's maximum capacity at saturation (mg/L). K_F is the Freundlich adsorption capacity parameter (mg/g) (L/mg). 1/n is the intensity parameter. R is the universal gas constant. T is the absolute temperature (K). b_T is Temkin isotherm constant. A_T is the binding constant (L/g). q_s, is the theoretical saturation capacity (mg/g). K_{ad} is the isotherm constant (mol^2/kJ^2).

2.4 | Thermodynamics of adsorption

The phrase adsorption thermodynamics refers to both the adsorption process itself and a method of detecting whether or not the adsorption process is practicable. Equation (10) can be used to compute variations in the adsorption free energy.

$$\Delta G = -RT \ln K_{eq}. \quad (10)$$

The change in Gibbs free energy is denoted by ΔG, while the equilibrium constant is denoted by K_{eq}. The natural logarithm of the pollution concentration in the solution at equilibrium (C_{Se}, mg/L) divided by the pollution concentration on the adsorbent at equilibrium (C_{Ae}, mg/L) and the inverse of the temperature gives the change in enthalpy and entropy (T and K), as given in Equation (11):

$$\ln \frac{C_{Se}}{C_{Ae}} = -\frac{\Delta H}{RT} + \frac{\Delta S}{R}. \quad (11)$$

The change in enthalpy of biosorption ($\Delta H°$) and the change in standard entropy ($\Delta S°$) are a function of the change in free energy ($\Delta G°$), as shown in Equation (12):

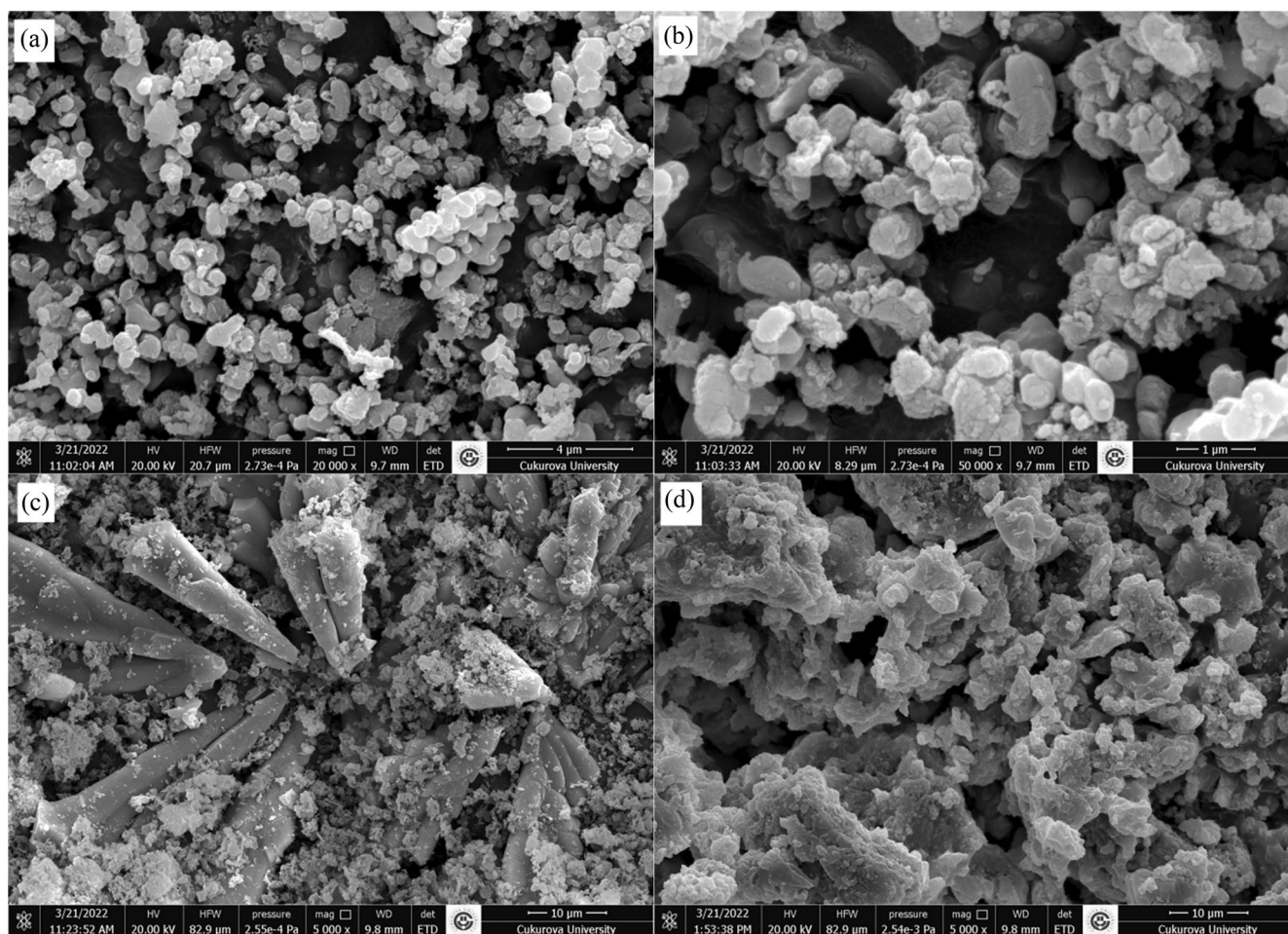$$\Delta G^o = \Delta H^o - T\Delta S^o. \quad (12)$$

FIGURE 2 SEM images of biosorbent; (a, b) Tomato stem ash images before adsorption process, (c) Tomato stem ash image after adsorption of DO 46 dye, and (d) Tomato stem ash image after PO_4^{3-} adsorption.

2.5 | Characterization of tomato stem ash for use as an adsorbent

The surface morphology of the biosorbent was determined by scanning electron microscopy (SEM; 20 kV, $2.18e^{-4}$ Pa). Energy dispersive x-ray (EDX) and Fourier transform infrared (FTIR) spectroscopy were used to evaluate the chemical components of the studied adsorbent before and after adsorption. For the principal components and minerals in the samples, x-ray fluorescence (XRF) was employed. In order to determine the surface charge of the biosorbent, zeta potential analysis (Malvern Zeta Sizer Nano ZS) was performed.

3 | RESULT AND DISCUSSION

3.1 | Characterization of tomato stem ash for use as an adsorbent

It is well knowledge that a biosorbent's photocatalytic activity is significantly influenced by the surface form of the material. Figure 2a, b show SEM images of the surface morphology of tomato stem ash. It is composed of hemispherical clusters of tomato stems that are roughly the same size and are scattered evenly. Figure 2c shows that the DO 46 dye has covered the surface of the tomato stem ash and the dye components have closed most of the pores on the external surface of the tomato stem. The image of the phosphate after the adsorption process is given in Figure 2d. It has been determined that it has denser layer structures than before phosphate adsorption.

Figure 3a shows the FTIR spectra of the biosorbent material before the adsorption procedure, which were recorded on a spectrophotometer. The presence of a biosorbent bond was revealed by a peak between 500 and 370 cm^{-1}.[30] S—S stretching was blamed for regions below 600 cm^{-1}. 1100–1000 cm^{-1} are a result of the strong bands of C—O group. Ionic carboxylic groups have a peak symmetric stretching vibration at 1409 cm^{-1}. It is due to acidic •OH groups stretching the 3700–2600 cm^{-1} vibration band. The top of the tomato stem ash exhibiting C—H stretch bonds (2987 cm^{-1}) was discovered.[31,32] The peaks in the FTIR spectrum of the biosorbent following dye adsorption (Figure 3b) reveal the presence of sulfur compound, with stretching at 602 cm^{-1} and 567 cm^{-1} indicating the presence of halogenated chemical. S═O at 1251 cm^{-1} represents the stretching of the sulfur compound. The reason why sulfur peaks are
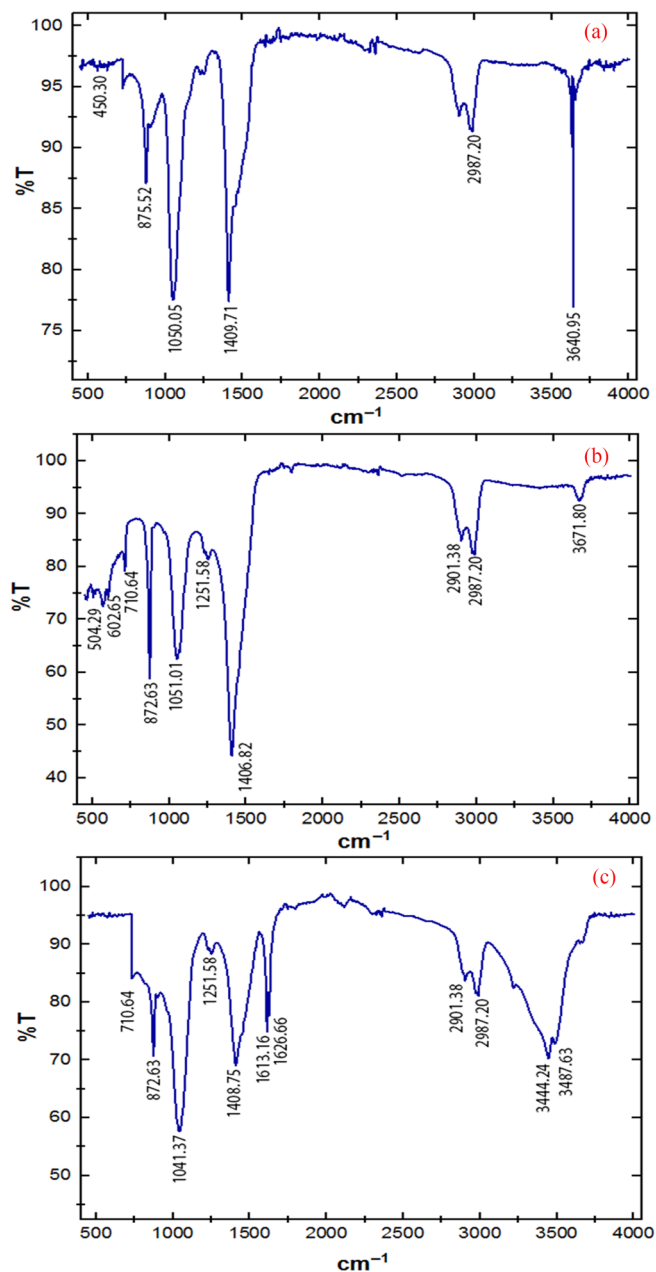
FIGURE 3 FTIR results of biosorbent (a) Tomato stem ash spectra before adsorption process, (b) Tomato stem ash spectra after adsorption of DO 46 dye, and (c) Tomato stem ash spectra after PO_4^{3-} adsorption.

seen after dye adsorption is the presence of sulfur in DO 46 dye. The benzene ring with two adjacent H atoms is shown by the peaks at 872 cm^{-1} and 710 cm^{-1}. It is interpreted as alkane C—H deformation at 1406 cm^{-1}. The azo character of amides was proved by N—H stretching at 2077 cm^{-1}. The bands around 2933–2960 cm^{-1} are most likely due to the presence of C—H stretching.[33,34]

In Figure 3c, the FTIR peaks of the adsorbent after phosphate adsorption are given. Frequencies in the range of 3650–3150 cm^{-1} are known as stretching vibrations originating from water molecules. The absence of two strong vibrations at 1626 cm^{-1} and 1613 cm^{-1} in

the pre-adsorption sample indicates that these two newly formed bands are symmetrical and asymmetrical vibrations found in the P—O bonds. In addition, the two weak vibrations occurring at 566 cm^{-1} and 599 cm^{-1} indicate O—P—O bonds, which are typical characteristic vibrations of P—O bonds.[35,36] Figure 4 shows the EDX outcomes of the biosorbent both before and after the adsorption process. According to the EDX spectra of tomato stem ash before adsorption process (Figure 4a), the weight-by-mass ratios of C, O, Mg, Si, and Ca elements were determined as 8.88%, 45.27%, 1.63%, 1.21%, and 43.02%, respectively.

Figure 4b shows the EDX results obtained after removal of the DO 46 dye. The weight ratios of C, O, Mg, Si, and Ca components were determined to be 7.58%, 48.83%, 2.79%, 0.6%, and 40.19%, respectively. The minerals present in the soil where the tomato stem ash grows are assumed to be the cause of the Mg and Si elements' presence in the bisorbent concentration.[37] Figure 4c illustrates EDX results of the bisorbent after the adsorption process of phosphate occurred. When the EDX results were examined, the weight percentages of O, Mg, Si, and Ca ions were obtained as 30.06%, 2.89%, 1.07%, and 31.5%, respectively. The values of Na and Cl elements in the EDX results were determined as 2.11% and 25.48%, respectively. After phosphate adsorption experiments on the surface of the biosorbent, a significant phosphorus (P, 6.74% w/w) peak was observed. In addition, the K ion was thought to come from the chemical $KH_2PO_4^{3-}$ used from the synthetically prepared phosphate solution. These findings show that the biosorbent adsorbs the phosphate contained in the water phase.

The compositions of the two materials were analyzed by XRF in both their unprocessed and sintering states to identify the constituents. The XRF results are shown in Table 2. The ratios of SiO_2 and Fe_2O_3 molecules did not change much, according to the XFR data. After sintering, the quantity of MgO increased significantly. This increase suggests that magnesium oxide is being produced in the material given that MgO sinters around 900°C. This is due to the material's conversion of $Mg(OH)_2$ to MgO as temperature increases.[38] The results showed that when the temperature was kept at a high level, the amount of SO_3 in the raw tomato stem composition increased. This situation could result from the raw material structure's sulfur-containing molecules, such SO_2, converting to SO_3 at high temperatures.[39]

The zeta potential and zeta potential of the biosorbent's surface charge were studied in relation to pH. The zeta potential results for evaluating potential charge interactions between DO 46, phosphate pollutants and biosorbent are shown in Figure 5. The zero charge point (PZC) or the isoelectric point are used to describe the electrical condition of an adsorbent surface in solution (IEP). PZC is defined as having a surface charge density of zero. The electrokinetic (ζ) potential in the shear plane is equal to zero, resulting in IEP.[40] The PZC changes in reaction to the net total (external and internal) surface charge of the adsorbent, whereas the IEP values clearly represent just the outer surface charge of the particles in solution.[41]

It was determined that the surface charge of the biosorbent was positive under acidic conditions. In a while, it was found that when

ELEMENT	Weight (%)
C	8.88
O	45.27
Mg	1.63
Si	1.21
Ca	43.02

ELEMENT	Weight (%)
C	7.58
O	48.83
Mg	2.79
Si	0.6
Ca	40.19

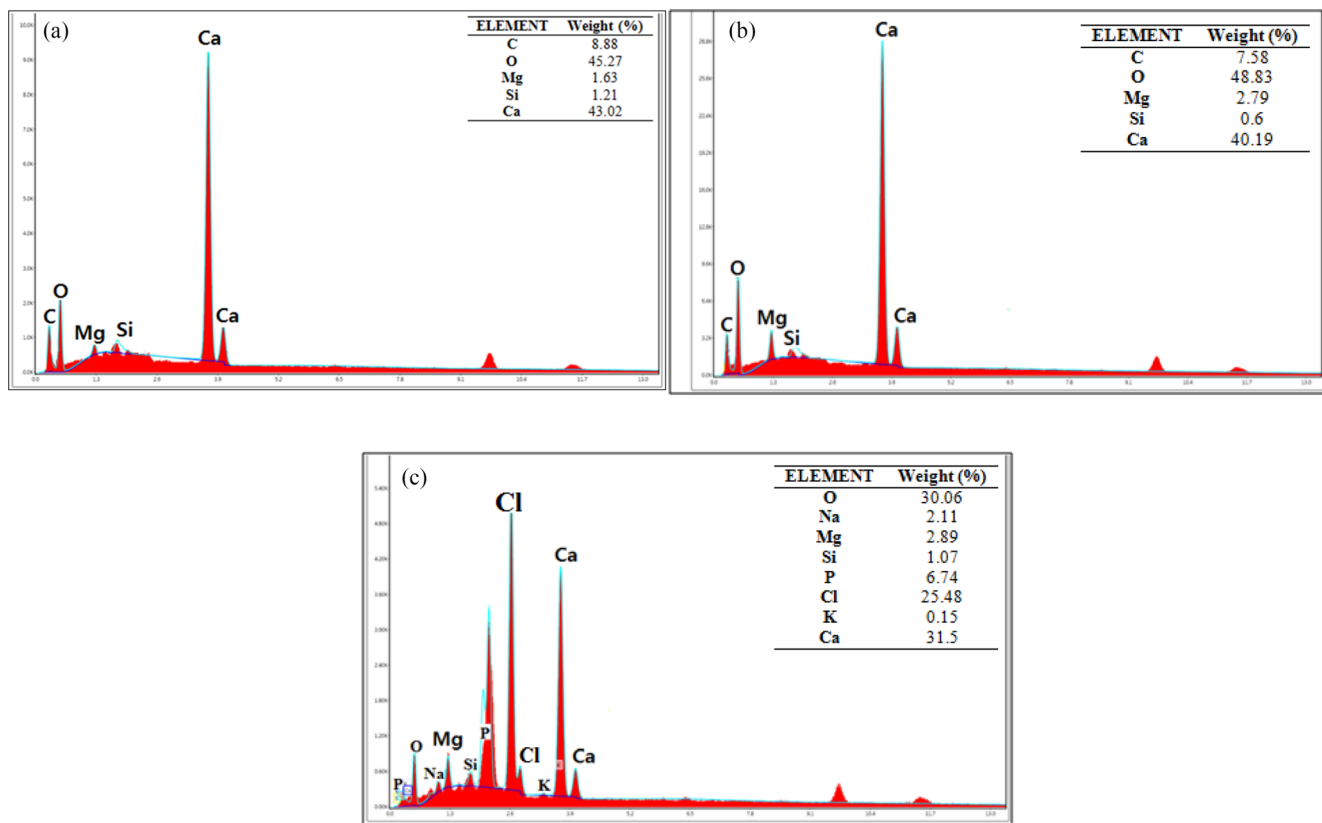| ELEMENT	Weight (%)
O	30.06
Na	2.11
Mg	2.89
Si	1.07
P	6.74
Cl	25.48
K	0.15
Ca	31.5

FIGURE 4 EDX results of biosorbent (a) Tomato stem ash spectra before adsorption process, (b) Tomato stem ash spectra after DO 46 dye adsorption, and (c) Tomato stem ash spectra after PO_4^{3-} adsorption.

TABLE 2 XRF results of tomato stem.

Materials Element	Raw tomato stem Dimension (%)	Tomato stem ash (after 900°C) Dimension (%)
Na_2O	0.11	0.60
MgO	1.55	7.65
SiO_2	0.35	0.39
SO_3	0.85	2.66
Fe_2O_3	0.39	0.20
CaO	26.94	67.93

the pH level increased, the biosorbent's surface charge changed from positive to negative. The biosorbent has a positive charge between pH 2 and pH 6, while the surface charge was negative up to pH 12.

3.2 | Results of adsorption experiments

3.2.1 | Effect of solution pH value on removal of PO_4^{3-} and DO 46 by adsorption process using tomato stem

The pH level controls protonation and deprotonation on the surface of the adsorbent. In this study, we focused at how the
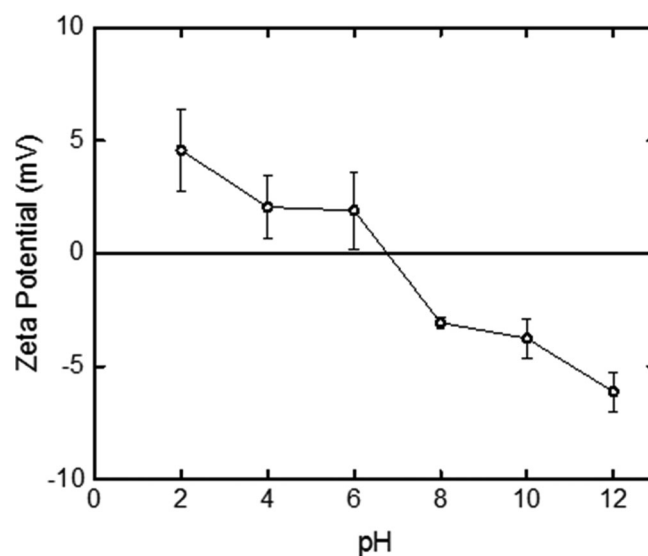

FIGURE 5 Zeta potential values of the biosorbent.

adsorbent affects pollutant removal using pH values of 2, 4, 6, 8, 10, and 12 (Figure 6). In order to examine the pH effect of phosphate in adsorption experiments, 1 g/L of adsorbent was added to the solution. Initial PO_4^{3-} concentration of 10 mg/L at room temperature for 1 h at a shaking speed of 150 rpm. The PO_4^{3-} adsorption
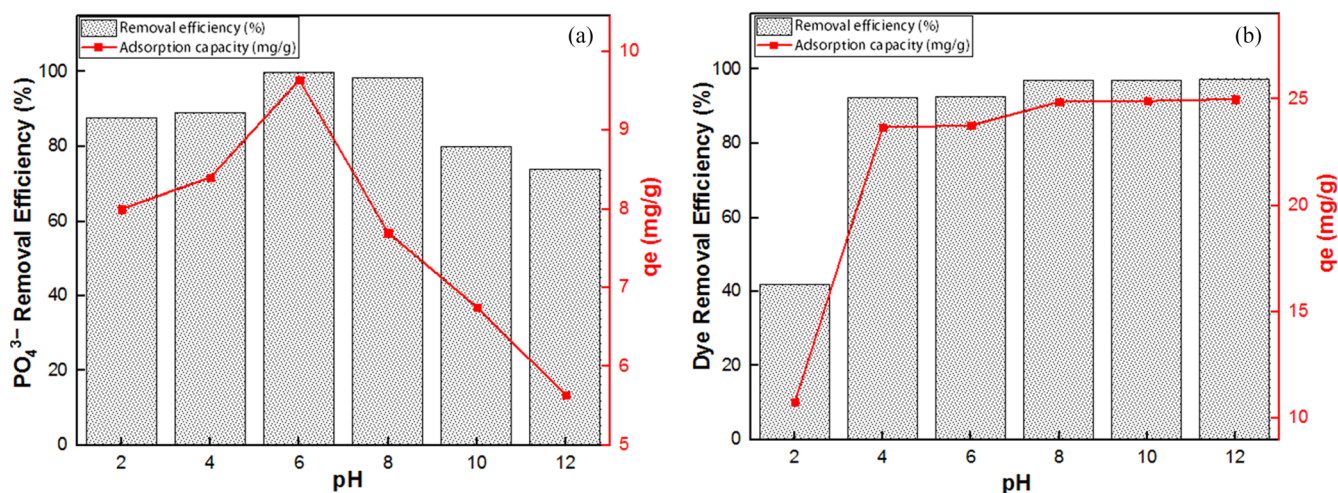
FIGURE 6   The effect of solution pH value on the adsorption process using tomato stem.

capacity increased as the pH of the solution raised, as shown in Figure 6a. However, after pH 6, the adsorbing capacity of the biosorbent gradually decreased. At pH 2, the removal effectiveness was 87.7%; however, at pH 6, the removal efficiency improved to 99.9%. The removal efficiency at pH 10 and pH 12 was determined to be 79.8% and 73.8%, respectively. This behavior can be interpreted according to the zeta potential results made within the scope of the study. At pH 6, the biosorbent's positive surface charge attracted the negatively charged chemical PO_4^{3-}, causing it to cling to the biosorbent's surface. The surface charge of the biosorbent, however, changed from positive to negative when the pH level shifted to a basic environment. This resulted in the repulsion of PO_4^{3-} with the same charge, which strengthened its adsorption. The adsorptive ability improved as the pH value increased in dye removal tests (Figure 6b). Using 1 g/L of adsorbent and an initial dye concentration of 25 mg/L, the solution was stirred at 150 rpm for 1 h at room temperature. At pH 2, the dye removal efficiency was 42%. When the pH increased to 4, the removal efficiency increased to 92.5%. The dye removal efficiency at pH 6, 8, 10, and 12 was determined as 92.8%, 97.1%, 97.3%, and 97.6%, respectively. When the dye removal efficiencies are compared, the pH 6 has been determined as the optimum condition for dye removal, considering that there is no significant difference between them and the consumption of chemicals to be used in pH adjustment.

3.2.2 | Effect of adsorbent dosage on removal of PO_4^{3-} and DO 46 by adsorption process using tomato stem ash

The effect of tomato stem ash dose on pollution removal efficiency was examined in this study. The adsorbent amounts for both types of pollutants were determined as 0.5, 0.75, 1, 1.5 and 2 g/L. The results of PO_4^{3-} removal efficiency with varying adsorbent dose are given in Figure 7a. Different amounts of adsorbent were added to the solution of

optimum pH value (pH 6) and initial concentration of PO_4^{3-} (10 mg/L) for 1 h. Increasing the biosorbent dosage resulted in a continuous increase in the PO_4^{3-} removal efficiency. In the experiments with 0.5, 1, and 2 g/L of adsorbent doses, PO_4^{3-} removal efficiency was determined as 77%, 86%, and 99%, respectively. The dye concentration was maintained at a constant at 25 mg/L while the adsorbent doses in the solution were increased (pH 12) (Figure 7b). The dye removal efficiency was 89.5% when using 0.5 g/L and 95% when using 1 g/L. The maximum removal effectiveness of DO 46 dye was reached by using 2 g/L of adsorbent dosage in this study, which was 98.7%. However, the calculated adsorbent capacity is expected to decrease as the adsorbent dosage increases. The reason behind is that as the amount of adsorbent increases, the amount of pollutant per adsorbent decreases. Therefore, the removal efficiency is supported by the adsorption capacity data.

3.2.3 | Effect of particle size on removal of PO_4^{3-} and DO 46 by adsorption process using tomato stem

The impact of biosorbent particle size on pollution removal was examined. In this study, three different adsorbent sizes (20 mesh, 30 mesh, and 35 mesh) were tested, as shown in Figure 8. The results of PO_4^{3-} adsorption experiments using different particle sizes are given in Figure 8a. PO_4^{3-} removal efficiencies were determined as 92.7%, 98.3%, and 99.2% for 20 mesh, 30 mesh, and 35 mesh, respectively. Adsorption capacity data suggest that as particle size decreased, adsorption capacity steadily increased. According to Figure 8b, where dye removal efficiencies are given, 98.5% of removal efficiency was obtained using 20 mesh particle size and 98.7% using 30 mesh particle size. However, the highest paint removal efficiency was obtained in 35 meshes as much as 90.5%. The dye adsorption capacity of tomato stem ash increased with decreasing particle size. As the particle size decreases, the surface area increases and effectively affects the adsorption of the pollutants.[42]
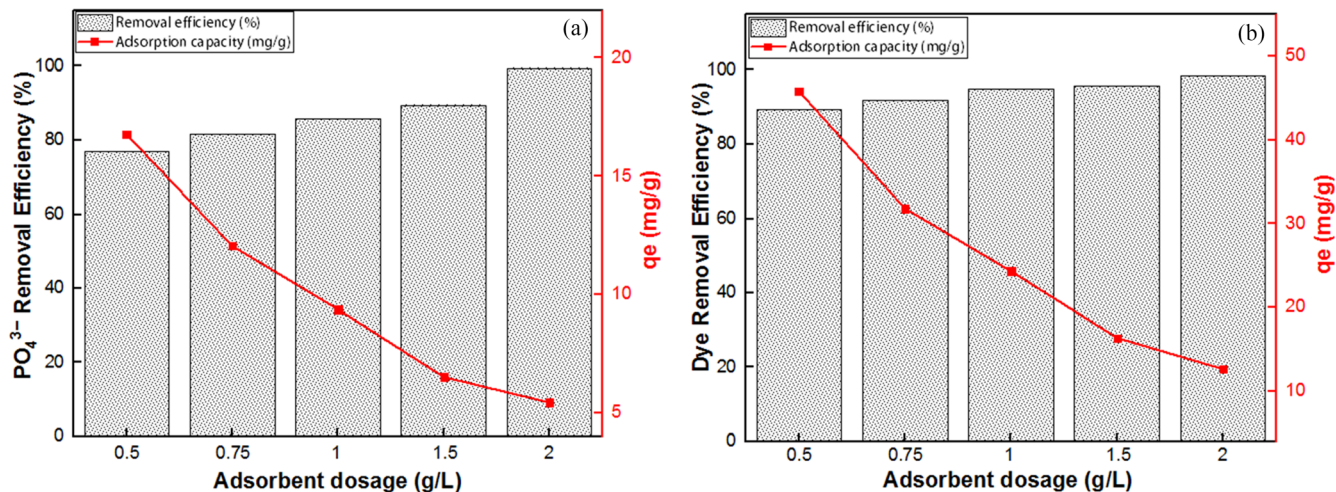
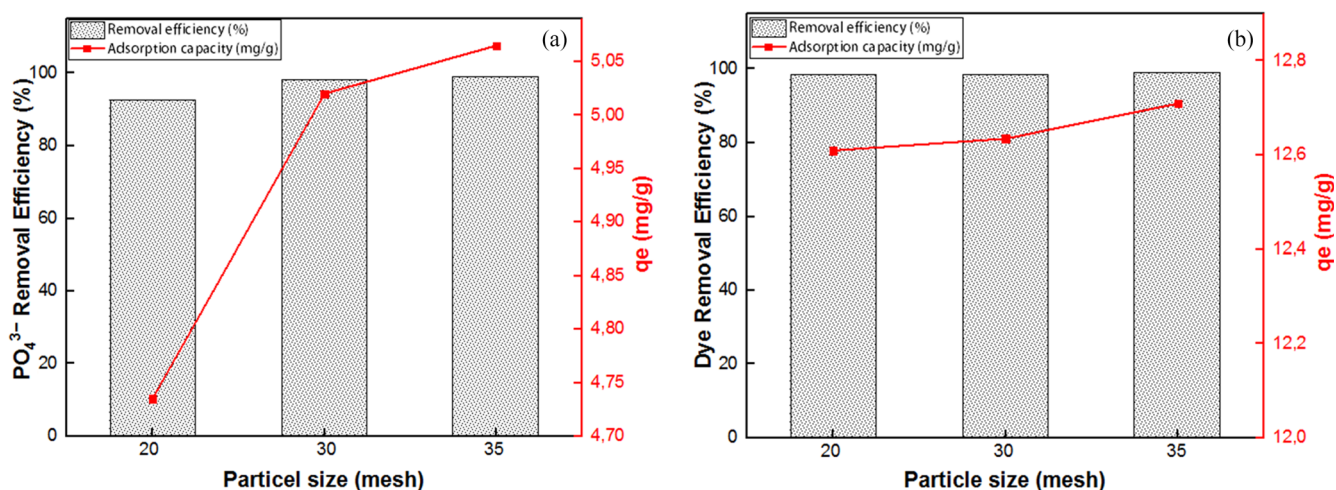**FIGURE 7**   The effect of adsorbent dosage on the adsorption process.

FIGURE 8   Effect of particle size on (a) PO_4^{3-} and (b) DO 46 dye removal efficiency and adsorption capacity.

3.2.4 | Effect of initial pollutant concentrations on removal of PO_4^{3-} and DO 46 by adsorption process using tomato stem

Figure 9 shows the findings of the initial pollutant concentration influence on the removal capability of pollutants using tomato stem. Initial concentrations of 10, 25, 50, and 75 mg/L for PO_4^{3-} were obtained from the stock solution (Figure 9a). According to the removal efficiency results of PO_4^{3-}, the removal efficiency increased with the increasing PO_4^{3-} concentration. The removal efficiencies of 10 mg/L, 25 mg/L and 50 mg/L initial concentration after 2 h of contact time were determined as 96.7%, 98.9%, and 99.3%, respectively. The capacity of tomato stems to absorb pollutants, on the other hand, increased as the pollutant concentration did. The rate of adsorbent dosage per unit and the quantity of pollutant grew gradually as the beginning concentration increased by keeping a constant amount of adsorbent in the environment. However, a slight decrease in removal efficiency was observed when the initial concentration was increased to 75 mg/L. This situation can be explained by the lack of sufficient amount of adsorbent to remove the quantity of pollutant in the environment.[43]

The initial dye concentration of DO 46 was varied for the following values: 25, 50, 100, and 200 mg/L and the obtained results are given in Figure 9b. The dye removal efficiency test findings revealed that the dye's removal effectiveness improved with increasing dye concentration. Initial dye concentrations of 25 mg/L and 50 mg/L had clearance efficiencies that were up to 99%, which was relatively comparable. The starting dye concentration was raised to 100 mg/L, but the clearance efficiency dropped to 98.3%. The removal efficiency was even decreased when the initial dye concentration was increased to 200 mg/L resulting in only 97% of removal efficiency. In the results obtained, an increase in direct proportion to the increase in the concentration of pollutants occurred with the use of tomato stem ash as an adsorbent.

3.2.5 | Kinetic studies

The adsorption kinetics of dye and phosphate were computed using the data given in this study. The coefficient of determination R^2 and kinetic parameters values of the different kinetics are given in Table 3.
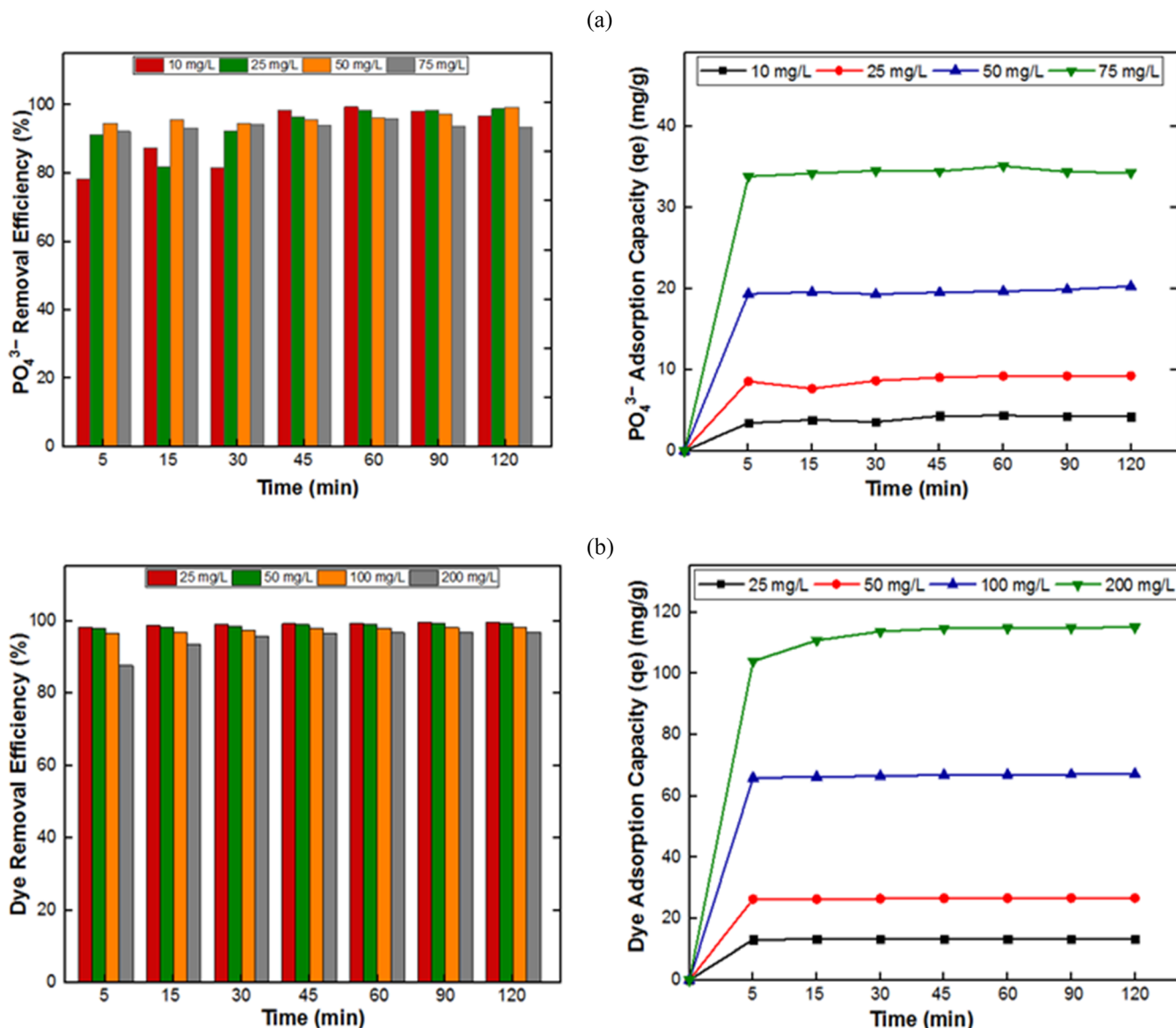
(a)

(b)

FIGURE 9 Effect of pollutant initial concentration on the removal efficiency and adsorption capacity of (a) PO_4^{3-} and (b) DO 46 dye.

Adsorption kinetics of pollutants will be determined according to the highest regression coefficient value (R^2). The closer R^2 value is to 1.00, the closer it is to the model and kinetics (in bold). [44,45]

The values of q_e and q_t from Table 3 represent the amount of DO 46 and PO_4^{3-} adsorbed on tomato stem ash adsorbent at equilibrium and at time t (min), respectively. [46,47] The pseudo-first-order kinetic, pseudo-second-order kinetic and intraparticle diffusion R^2 for DO 46 dye were found to be with good correlation coefficient: 0.97, 1.00, and 0.96, respectively. According to the obtained results, DO 46 dye adsorption on tomato stems adsorbent is more suitable for pseudo-second-order kinetic with the highest R^2 value. According to the adsorption kinetic studies of PO_4^{3-}, the R^2 of the pseudo-first-order kinetic model was 0.66, the R^2 of the pseudo-second-order kinetic model was 0.97, and the R^2 of the intraparticle diffusion was calculated as 0.58. Therefore, PO_4^{3-} adsorption has also followed the pseudo-second-order kinetic model. The application of the

pseudo-second-order kinetic model suggests that DO 46 dye and PO_4^{3-} adsorption on tomato stem ash was based on a chemical adsorption involving electron exchange between adsorbent and adsorbate. [48] Furthermore, these findings demonstrate the functioning of the adsorption process as well as the quick transfer of DO 46 dye and PO_4^{3-} to the surface as a result of the availability of uncoated surface area. [49]

3.2.6 | Adsorption isotherm

One of the most significant adsorption approaches for predicting adsorbent–adsorbate interactions, analyzing the biosorption mechanism, and measuring adsorbent adsorption capacity is isotherm analysis. [50] The results of the adsorption isotherm calculations are given in Table 4.

The R^2 values for the Langmuir isotherm were 0.9319, 0.9496 for Freundlich isotherm, 0.4394 for Temkin isotherm, and 0.9479 for

D–R isotherm, which were determined as a result of the absorption of DO 46 dye on tomato stem ash adsorbent. Therefore, according to the obtained R^2 values, it was determined that the highest coefficient corresponds to Freundlich isotherm meaning it was the appropriate isotherm describing the adsorbing of DO 46 dye on tomato stem. The R^2 value of the Freundlich isotherm of PO_4^{3-} was 0.7432, while the R^2 value of the D–R isotherm was calculated as 0.9302. However, the Temkin isotherm of PO_4^{3-} has a greater correlation coefficient (0.9906) than the Langmuir isotherm (0.9335). Thus, the adsorption of PO_4^{3-} onto the tomato stem ash was described by the Temkin isotherm. All adsorption sites must be energetically equal and similarly homogenous, according to the Langmuir model. Due to the multilayer adsorption mechanism, the adsorption process heterogeneity is connected to the Freundlich isotherm model. For the adsorption of contaminants on the adsorbent, the Temkin model includes the interaction between adsorbent and adsorbate. The D–R isotherm is widely used to describe the physical or chemical nature of the sorption process and the pore-filling mechanism.[51–53] The fact that DO 46 dye was attached to the Freundlich isotherm indicates that it is adsorbed on the tomato stem ash in a multilayer heterogeneous adsorption type.[54,55] The electrostatic attraction of opposite charged molecules is explained by the fact that PO_4^{3-} was connected to the D–R isotherm in this study.

3.2.7 | Adsorption thermodynamic

In this study, thermodynamic experiments were carried out to determine the effect of temperature on the removal of pollutants on the tomato stem ash (Table 5). The thermodynamic quantities were calculated for the adsorption of DO 46 and PO_4^{3-} on tomato stem ash and the results were summarized in Table 5. Parameters called enthalpy and entropy express important situations that should be considered in the adsorption process depending on thermodynamics.[56]

From Table 5, the calculated Gibbs free energy of DO 46 dye was negative; which indicates that the adsorption of dye onto the adsorbent is possible and spontaneous in nature.[57,58] In addition, negative ΔH indicates that the adsorption of DO 46 dye is exothermic.[59] According to the thermodynamic results of PO_4^{3-}, it is understood that the adsorption is spontaneous with the negative ΔG° values, and the adsorption is endothermic with a positive ΔH°.[60] Positive values of entropy change ΔS° indicate the stability of the solution interface during the adsorption for both studied adsorption systems.[61,62]

4 | COMPARE WITH OTHER STUDIES

In this study, DO 46 dye and phosphate removal were studied using tomato biosorbent. In these adsorption processes, adsorption capacities of 13.76 and 4.24 mg/g, respectively. Removal efficiencies of 99.44% and 99.31% were achieved (Table 6). In addition, it was found that the dye DO 46 followed the cautious isotherm, had pseudo-second-order kinetics, and the adsorption process was exothermic. It was concluded that in the phosphate adsorption process, it follows the D–R isotherm, belongs to the pseudo-second-order kinetics, and the process is endothermic. In addition, Table 6 shows that our study looks in more detail at DO 46 uptake when compared to the previous studies.

TABLE 3 Adsorption kinetics results of DO 46 and PO_4^{3-} removal using tomato stem.

Kinetics	Parameters	DO 46	PO_4^{3-}
Pseudo-first-order	K_1 (min^{-1})	0.039	0.068
	q_e (mg/g)	0.601	1.76
	R^2	0.9746	0.664
Pseudo-second-order	K_2 (g/mg.min)	0.019	0.096
	q_e (mg/g)	26.74	4.28
	R^2	1	0.9763
Intraparticle diffusion	K_p	0.056	0.1522
	C	26.18	3.058
	R^2	0.9601	0.5836

TABLE 4 Isotherm parameters for adsorption of PO_4^{3-} and DO 46 on tomato stem.

Isotherm	Parameters	DO 46	PO_4^{3-}
Langmuir	K_L	68.22	0.2
	Q_{max} (mg/g)	16.28	16.69
	R^2	0.9319	0.9335
Freundlich	K_f (mg/g)	664.04	36.08
	$1/n$ (g/L)	1.009	0.45
	R^2	0.9496	0.7432
Temkin	RT/b (g/L)	47.40	552.38
	K_T	3074.89	3.24
	R^2	0.4394	0.9906
D-R	K_{DR} (mol^2 kJ^{-2})	0.0046	0.0008
	Q_{DR} (mg g^{-1})	55.19	3.29
	R^2	0.9479	0.9302

TABLE 5 Adsorption thermodynamic results of tomato stem ash used as adsorbent.

Temperature (°K)	Direct Orange			PO_4^{3-}		
	ΔG (KJ.mol^{-1})	ΔH	ΔS	ΔG (KJ.mol^{-1})	ΔH	ΔS
303	−8.41133	−3.174	0.0173	−5.21309	5.7357	0.0361
313	−8.60354			−5.56293		
323	−8.75658			−5.93604		

TABLE 6 Comparison with other studies.

Adsorbate	Adsorbent	Adsorbent capacity (mg/g)	Removal Efficiency (%)	Isotherm	Kinetic	Thermodynamic	References
DO 46	TS	13.76	99.44	Temkin	Pseudo-second order	Exothermic	This study
PO_4^{3--}	TS	4.24	99.31	D-R	Pseudo-second order	Endothermic	This study
DO 46	Cationized cotton	31.28	–	Langmuir	–	Exothermic	63
DO 46	Bleached cotton	42.73	–	Freundlich	–	Exothermic	63
PO_4^{3-}	Tobacco stem biochar	2.55	–	Freundlich	Pseudo-second order	–	64
Congo Red	*Cornulaca monacantha* stem	–	86.3	Langmuir	Elovic	Endothermic	65
Crystal Viyole	Apple stem	153.85	96.0	Langmuir	Pseudo-second order	Endothermic	66
Methylene Blue	Maize stem	160.84	99.9	Freundlich	Pseudo-second order	–	67
Eriochrome black T	Maize stem	167.1	66.8	Langmuir	Pseudo-second order	–	67

5 | CONCLUSION

Adsorbents obtained from natural materials have gained importance in the last decade. In this study, it was synthesized an adsorbent without adding any chemical material to the tomato stem. The obtained biosorbent was used for dye and phosphate removal in the adsorption process. For DO 46 dye with an initial concentration of 200 mg/L and at optimum conditions (pH: 12, adsorbent dosage: 2 g/L, particle size: 600 μm, contact time: 120 min.) 99.44% of removal efficiency and equivalent of 13.76 mg/g adsorption capacity were determined. In the adsorption experiments of phosphate, 2 g/L adsorbent (600 μm) was added to the solution with an initial concentration of 50 mg/L and a pH value of 6, and 120 min of agitation time to obtain a removal efficiency of 99.31% (4.24 mg/g of adsorption capacity). As a result of the characterization analyzes (SEM, FTIR, and EDX) performed on the biosorbent before and after adsorption, it was proven that the impurities were adsorbed effectively on the adsorbent surface. As a result of XRF performed before adsorption, the content of tomato stem ash was determined. According to the zeta potential, the bisorbent has a positive surface charge up to a pH of 6, but when the pH rises, the surface charge becomes negative. Besides, the Freundlich isotherm (R^2: 0.94) was the most suitable to explain the relationship between DO 46 dye and adsorbent. The most suitable isotherm for the adsorption of PO_4^{3-} by tomato stem ash was the Temkin isotherm (R^2: 0.99). The pseudo-second-order kinetic model was discovered to be the most accurate one for both pollutants. It was discovered that the spontaneous exothermic process of DO 46 dye adsorption occurs in contrast to the spontaneous endothermic process of PO_4^{3-} adsorption. According to the obtained results within the scope of this study, it has been determined that tomato stem ash adsorbent is suitable to be used for dye and phosphate removal in the adsorption process. However, with promoting technology and improved steps, promising results can be obtained for the removal of wider pollutants using the processed biosorbent.

AUTHOR CONTRIBUTIONS

Ozan Eskikaya: Methodology; writing – original draft. **Hudaverdi Arslan:** Writing – original draft; writing – review and editing. **Melis Gun:** Data curation; methodology. **Raouf Bouchareb:** Methodology; writing – original draft; writing – review and editing. **Nadir Dizge:** Investigation; writing – original draft; writing – review and editing.

CONFLICT OF INTEREST STATEMENT

The authors declare that they have no competing interests.

DATA AVAILABILITY STATEMENT

The datasets created and/or analyzed during the current investigation are accessible upon reasonable request from the corresponding author.

ORCID

Ozan Eskikaya https://orcid.org/0000-0002-8470-4341
Nadir Dizge https://orcid.org/0000-0002-7805-9315

REFERENCES

1. Khan SAR, Ponce P, Yu Z, Golpîra H, Mathew M. Environmental technology and wastewater treatment: strategies to achieve environmental sustainability. *Chemosphere*. 2022;286:131532.
2. Mao G, Han Y, Liu X, Crittenden J, Huang N, Ahmad UM. Technology status and trends of industrial wastewater treatment: a patent analysis. *Chemosphere*. 2022;288:132483.
3. Recepoglu YK, Goren AY, Orooji Y, Khataee A. Carbonaceous materials for removal and recovery of phosphate species: limitations, successes and future improvement. *Chemosphere*. 2022;287:132177.
4. Moumen E, Bazzi L, El Hankari S. Aluminum-fumarate based MOF: a promising environmentally friendly adsorbent for the removal of phosphate. *Process Safety Environ Protect*. 2022;160:502-512.
5. Bilici Z, Bouchareb R, Sacak T, Yatmaz HC, Dizge N. Recycling of TiO_2-containing waste and utilization by photocatalytic degradation of a reactive dye solution. *Water Sci Technol*. 2021;83(5):1242-1249.
6. Bouchareb R, Bilici Z, Dizge N. Potato processing wastewater treatment using a combined process of chemical coagulation and membrane filtration. *CLEAN*. 2021;49(11):2100017.

7. Henning LM, Simon U, Abdullayev A, et al. Effect of fomes fomentarius cultivation conditions on its adsorption performance for anionic and cationic dyes. *ACS Omega*. 2022;7(5):4158-4169.

8. Oukebdane K, Necer IL, Didi MA. Binary comparative study adsorption of anionic and cationic azo-dyes on Fe_3O_4-bentonite magnetic nanocomposite: kinetics, equilibrium. *Mech Thermodyn Study Silicon*. 2022;14:1-14.

9. Zhang Y, Hui C, Wei R, et al. Study on anionic and cationic dye adsorption behavior and mechanism of biofilm produced by bacillus amyloliquefaciens DT. *Appl Surf Sci*. 2022;573:151627.

10. Kim S, Nam SN, Jang A, et al. Review of adsorption–membrane hybrid systems for water and wastewater treatment. *Chemosphere*. 2022;286:131916.

11. Jabbar KQ, Barzinjy AA, Hamad SM. Iron oxide nanoparticles: preparation methods, functions, adsorption and coagulation/flocculation in wastewater treatment. *Environ Nanotechnol Monitor Manage*. 2022;17:100661.

12. Bouchareb R, Bilici Z, Dizge N. Water recovery from yarn fabric dyeing wastewater using electrochemical oxidation and membrane processes. *Water Environ Res*. 2022;94(1):e1681.

13. Goh PS, Wong KC, Ismail AF. Membrane technology: a versatile tool for saline wastewater treatment and resource recovery. *Desalination*. 2022;521:115377.

14. Shkir M, Palanivel B, Khan A, et al. Enhanced photocatalytic activities of facile auto-combustion synthesized ZnO nanoparticles for wastewater treatment: an impact of Ni doping. *Chemosphere*. 2022;291:132687.

15. Eskikaya O, Ozdemir S, Tollu G, et al. Synthesis of two different zinc oxide nanoflowers and comparison of antioxidant and photocatalytic activity. *Chemosphere*. 2022;306:135389.

16. Hassani A, Malhotra M, Karim AV, Krishnan S, Nidheesh PV. Recent progress on ultrasound-assisted electrochemical processes: a review on mechanism, reactor strategies, and applications for wastewater treatment. *Environ Res*. 2022;205:112463.

17. Kamaraj R, Davidson DJ, Sozhan G, Vasudevan S. Adsorption of herbicide 2-(2,4-dichlorophenoxy)propanoic acid by electrochemically generated aluminum hydroxides: an alternative to chemical dosing. *RSC Adv*. 2015;5:39799-39809.

18. Vieira Y, Netto MS, Lima ÉC, Anastopoulos I, Oliveira ML, Dotto GL. An overview of geological originated materials as a trend for adsorption in wastewater treatment. *Geosci Front*. 2022;13(1):101150.

19. Pandiarajan A, Kamaraj R, Vasudevan S. Enhanced removal of cephalosporin based antibiotics (CBA) from water by one-pot electrosynthesized $Mg(OH)_2$: a combined theoretical and experimental study to pilot scale. *New J Chem*. 2017;41:4518-4530.

20. Kamaraj R, Davidson DJ, Sozhan G, Vasudevan S. Adsorption of 2,4-dichlorophenoxyacetic acid (2,4-D) from water by in situ generated metal hydroxides using sacrificial anodes. *J Taiwan Inst Chem Eng*. 2014;45:2943-2949.

21. Costa TC, Hendges LT, Temochko B, et al. Evaluation of the technical and environmental feasibility of adsorption process to remove water soluble organics from produced water: a review. *J Petrol Sci Eng*. 2022;208:109360.

22. Baskar AV, Bolan N, Hoang SA, et al. Recovery, regeneration and sustainable management of spent adsorbents from wastewater treatment streams: a review. *Sci Total Environ*. 2022;822:153555.

23. Sultana M, Rownok MH, Sabrin M, Rahaman MH, Alam SN. A review on experimental chemically modified activated carbon to enhance dye and heavy metals adsorption. *Clean Eng Technol*. 2022;6:100382.

24. Chen Z, Li Z, Chen J, Tan H, Wu J, Qiu H. Selective adsorption of rare earth elements by Zn-BDC MOF/graphene oxide nanocomposites synthesized via in situ interlayer-confined strategy. *Ind Eng Chem Res*. 2022;61:1841-1849.

25. Peng Y, Li Y, Liu L, et al. New optimization approach for amphoteric/magnetic ramie biosorbent in dyestuff adsorption. *Biochem Eng J*. 2022;181:108379.

26. Deniz F, Tezel Ersanli E. A novel biowaste-based biosorbent material for effective purification of methylene blue from water environment. *Int J Phytoremediation*. 2022;24:1-8.

27. Rice EW, Baird RB, Eaton AD. *Standard Methods for the Examination of Water and Wastewater*. 23rd ed. American Public Health Association, American Water Works Association, Water Environment Federation; 2017 ISBN: 9780875532875.

28. Aniagor CO, Igwegbe CA, Ighalo JO, Oba SN. Adsorption of doxycycline from aqueous media: a review. *J Mol Liq*. 2021;334:116124.

29. Largitte L, Pasquier R. A review of the kinetics adsorption models and their application to the adsorption of lead by an activated carbon. *Chem Eng Res Design*. 2016;109:495-504.

30. Nadeem F, Bhatti IA, Ashar A, et al. Eco-benign biodiesel production from waste cooking oil using eggshell derived MMCaO catalyst and condition optimization using RSM approach. *Arab J Chem*. 2021;14(8):103263.

31. Alkanan ZT, Al-Hilphy AR, Altemimi AB, Mandal R, Pratap-Singh A. Comparison of quality characteristics of tomato paste produced under ohmic-vacuum combination heating and conventional heating. *Appl Food Res*. 2021;1(2):100014.

32. Vorobyova V, Skiba M, Vasyliev G. Extraction of phenolic compounds from tomato pomace using choline chloride–based deep eutectic solvents. *J Food Measure Character*. 2022;16(2):1087-1104.

33. Jadhav JP, Phugare SS, Dhanve RS, Jadhav SB. Rapid biodegradation and decolorization of direct Orange 39 (Orange TGLL) by an isolated bacterium Pseudomonas aeruginosa strain BCH. *Biodegradation*. 2010;21(3):453-463.

34. Srinivasan P, Bosco AJ, Kalaivizhi R, Selvi JA, Sivakumar P. Adsorption isotherm and kinetic study of Direct Orange 102 dyes on TNJ activated carbon. *Mater Today Proc*. 2021;34:389-394.

35. Zhang L, Liu Y, Wang Y, Li X, Wang Y. Investigation of phosphate removal mechanisms by a lanthanum hydroxide adsorbent using p-XRD. *FTIR XPS Appl Surf Sci*. 2021;557:149838.

36. Kumar IA, Jeyaseelan A, Viswanathan N, Naushad M, Valente AJ. Fabrication of lanthanum linked trimesic acid as porous metal organic frameworks for effective nitrate and phosphate adsorption. *J Solid State Chem*. 2021;302:122446.

37. Epihov DZ, Saltonstall K, Batterman SA, et al. Legume–microbiome interactions unlock mineral nutrients in regrowing tropical forests. *Proc Natl Acad Sci*. 2021;118(11):e2022241118.

38. Rani N, Chahal S, Kumar P, Kumar A, Shukla R, Singh SK. MgO nanostructures at different annealing temperatures for d0 ferromagnetism. *Vacuum*. 2020;179:109539.

39. Moodley C, Naidoo N, Moodley S, Carsky M, Lokhat D. Effects of SO_3 formation on high temperature flue gas desulphurization performance. South African journal of. *Chem Eng*. 2022;40:107-112.

40. Vasudevan S, Oturan MA. Electrochemistry: as cause and cure in water pollution-an overview. *Environ Chem Lett*. 2014;12:97-108.

41. Saleh M, Isik Z, Arslan H, Yalvac M, Dizge N. Adsorption of phosphate ions from aqueous solutions using marble, pumice, and basalt triple combination. *Water Air Soil Pollut*. 2022;233(6):181.

42. Saleh M, Isik Z, Yabalak E, Yalvac M, Dizge N. Green production of hydrochar nut group from waste materials in subcritical water medium and investigation of their adsorption performance for crystal violet. *Water Environ Res*. 2021;93(12):3075-3089.

43. Isik Z, Saleh M, M'barek I, Yabalak E, Dizge N, Deepanraj B. Investigation of the adsorption performance of cationic and anionic dyes using hydrochared waste human hair. *Biomass Convers Biorefin*. 2022;12:1-14.

44. Vasudevan S, Lakshmi J. Electrochemical removal of boron from water: adsorption and thermodynamic studies. *Can J Chem Eng*. 2012;90:1017-1026.

45. De Clercq J, Van De Steene E, Verbeken K, Verhaege M. Electrochemical oxidation of 1,4-dioxane at boron-doped diamond electrode. *J Chem Technol Biotechnol*. 2010;85:1162-1167.

46. Kamaraj R, Pandiarajan A, Jayakiruba S, Naushad M, Vasudevan S. Kinetics, thermodynamics and isotherm modeling for removal of nitrate from liquids by facile one-pot electrosynthesized nano zinc hydroxide. *J Mol Liq*. 2016;215:204-211.

47. Kamaraj R, Vasudevan S. Facile one-pot synthesis of nano-zinc hydroxide by electro-dissolution of zinc as a sacrificial anode and the application for adsorption of Th4+, U4+, and Ce4+ from aqueous solution. *Res Chem Intermed*. 2016;42:4077-4095.

48. Abbou B, Lebkiri I, Ouaddari H, et al. Removal of Cd (II), Cu (II), and Pb (II) by adsorption onto natural clay: a kinetic and thermodynamic study. *Turk J Chem*. 2021;45(2):362-376.

49. Hasani N, Selimi T, Mele A, et al. Theoretical, equilibrium, kinetics and thermodynamic ınvestigations of methylene blue adsorption onto lignite coal. *Molecules*. 2022;27:1856.

50. Gemici BT, Ozel HU, Ozel HB. Removal of methylene blue onto forest wastes: adsorption isotherms, kinetics and thermodynamic analysis. *Environ Technol Innov*. 2021;22:101501.

51. Tariq S, Saeed M, Zahid U, et al. Green and eco-friendly adsorption of dyes with organoclay: isothermal, kinetic and thermodynamic studies. *Toxin Rev*. 2021;41(4):1-10.

52. Chakraborty S, Mukherjee A, Das S, Maddela NR, Iram S, Das P. Study on isotherm, kinetics, and thermodynamics of adsorption of crystal violet dye by calcium oxide modified fly ash. *Environ Eng Res*. 2021;26 (1):190372.

53. Aslani CK, Amik O. Active carbon/PAN composite adsorbent for uranium removal: modeling adsorption isotherm data, thermodynamic and kinetic studies. *Appl Radiat Isot*. 2021;168:109474.

54. Vasudevan S, Lakshmi J, Sozhan G. Electrocoagulation studies on the removal of copper from water using mild steel electrode. *Water Environ Res*. 2012;84:209-219.

55. Ganesan P, Lakshmi J, Sozhan G, Vasudevan S. Removal of manganese from water by electrocoagulation: adsorption, kinetics and thermodynamic studies. *Can J Chem Eng*. 2013;91:448-458.

56. Bachmann SAL, Calvete T, Féris LA. Caffeine removal from aqueous media by adsorption: an overview of adsorbents evolution and the kinetic, equilibrium and thermodynamic studies. *Sci Total Environ*. 2021;767:144229.

57. Vasudevan S, Lakshmi J, Sozhan G. Optimization of the process parameters for the removal of phosphate from drinking water by electrocoagulation. *Desalin Water Treat*. 2009;12:407-414.

58. Pandiarajan A, Kamaraj R, Vasudevan S, Vasudevan S. OPAC (orange peel activated carbon) derived from waste orange peel for the adsorption of chlorophenoxyacetic acid herbicides from water:

adsorption isotherm, kinetic modelling and thermodynamic studies. *Bioresour Technol*. 2018;261:329-341.

59. Saeed T, Naeem A, Din IU, et al. Synthesis of chitosan composite of metal-organic framework for the adsorption of dyes; kinetic and thermodynamic approach. *J Hazard Mater*. 2022;427:127902.

60. Koçkaya G. Anilin Mavisinin Atıksulardan Uzaklaştırılmasında Yeni Bir Adsorbent Kullanımı. Dissertation. Fen Bilimleri Enstitüsü. 2016.

61. Oukebdane K, Necer IL, Didi MA. Binary comparative study adsorption of anionic and cationic azo-dyes on Fe_3O_4-bentonite magnetic nanocomposite: kinetics, equilibrium, mechanism and thermodynamic study. *Silicon*. 2022;14:1-14.

62. Vasudevan S, Jayaraj J, Lakshmi J, Sozhan G. Removal of iron from drinking water by electrocoagulation: adsorption and kinetics studies. *Korean J Chem Eng*. 2009;26:1058-1064.

63. Khanjani Y, Farizadeh K, Ahmadi S. Improve of direct dye (Direct Orange 46) sorption on pretreated cotton fabric by cationic agent. 2011.

64. Yi M, Chen Y. Enhanced phosphate adsorption on Ca-Mg-loaded biochar derived from tobacco stems. *Water Sci Technol*. 2018;78(11): 2427-2436.

65. Sharma A, Siddiqui ZM, Dhar S, Mehta P, Pathania D. Adsorptive removal of Congo red dye (CR) from aqueous solution by Cornulaca monacantha stem and biomass-based activated carbon: isotherm, kinetics and thermodynamics. *Sep Sci Technol*. 2019;54(6):916-929. doi:10.1080/01496395.2018.1524908

66. Takabi AS, Shirani M, Semnani A. Apple stem as a high performance cellulose based biosorbent for low cost and eco-friendly adsorption of crystal violet from aqueous solutions using experimental design: mechanism, kinetic and thermodynamics. *Environ Technol Innov*. 2021; 24:101947.

67. Vučurović VM, Razmovski RN, Miljić UD, Puškaš VS. Removal of cationic and anionic azo dyes from aqueous solutions by adsorption on maize stem tissue. *J Taiwan Inst Chem Eng*. 2014;45(4):1700-1708.